Atmos. Chem. Phys., 11, 9595–9603, 2011
www.atmos-chem-phys.net/11/9595/2011/
doi:10.5194/acp-11-9595-2011

Atmospheric Chemistry and Physics

The observation of chemiluminescent NiO* emissions in the laboratory and in the night airglow

W. F. J. Evans[1,2], R. L. Gattinger[3], A. L. Broadfoot[4], and E. J. Llewellyn[3]

[1]Northwest Research Associates Inc., 4118 148 Avenue N.E., Redmond, WA 98052, USA
[2]Centre for Research in Earth and Space Science, York University, 4700 Keele Street, Toronto, ON M3J 1P3, Canada
[3]ISAS, Department of Physics and Engineering Physics, 116 Science Place, University of Saskatchewan, Saskatoon, SK S7N 5E2, Canada
[4]Lunar and Planetary Laboratory, University of Arizona, 1629 E. University Blvd., Tucson, AZ 85721-0092, USA

Received: 18 March 2011 – Published in Atmos. Chem. Phys. Discuss.: 15 April 2011
Revised: 19 July 2011 – Accepted: 21 August 2011 – Published: 16 September 2011

Abstract. The recent finding of an orange spectral feature in OSIRIS/Odin spectra of the night airglow near 87 km has raised interest in the origin of the emission. The feature was positively identified as the chemiluminescent FeO* emission where the iron is of meteoric origin. Since the meteorite source of atomic metals in the mesosphere contains both iron and nickel, with Ni being typically 6 % of Fe, it is expected that faint emissions involving Ni should also be present in the night airglow. The present study summarizes the laboratory observations of chemiluminescent NiO* emissions and includes a search for the NiO* signature in the night airglow. A very faint previously unidentified "continuum" extending longwave of 440 nm has been detected in the night airglow spectra obtained with two space-borne limb viewing instruments. Through a comparison with laboratory spectra this continuum is identified as arising from the NiO* emission. The altitude profile of the new airglow emission has also been measured. The similarity of the altitude profiles of the FeO* and NiO* emissions also suggests the emission is NiO as both can originate from reaction of the metal atoms with mesospheric ozone. The observed NiO* to FeO* ratio exhibits considerable variability; possible causes of this observed variation are briefly discussed.

Correspondence to: E. J. Llewellyn
(edward.llewellyn@usask.ca)

1 Introduction

The terrestrial night airglow has been studied for more than a century (e.g. Ångström, 1869). However, new emission features are still being identified, an example being the FeO "orange" bands that arise from the reaction between atomic iron of meteoric origin with terrestrial ozone (Evans et al., 2010). Known emission features continue to be investigated and their spectral signatures more accurately determined; such as the chemiluminescent emission of NO_2^* that is produced in the NO + O reaction (Becker et al., 1972; Gattinger et al., 2010). Extending these ongoing observations, it is expected that a chemiluminescent emission from NiO*, which also arises from the reaction of atomic nickel of meteoric origin (McNeil et al., 1998) with atmospheric ozone, should be present in the airglow spectrum, albeit very faint.

At least two NiO* band systems are known to be present in the visible spectral region, the NiO "blue" bands in the 500 nm region (Srdanov and Harris, 1988) and the "red" $^3\Sigma^- - X^3\Sigma^-$ system that occurs in the 620 nm region (Friedman-Hill and Field, 1992). Due to the complexity of the spectra the determination of the molecular constants for the upper electronic states is challenging and consequently the definitive assignment of vibrational transitions remains incomplete. Srdanov and Harris (1988) did publish a laboratory spectrum of chemiluminescent NiO* over the 480 to 600 nm wavelength range and more recently Burgard et al. (2006) obtained the spectrum over a much broader wavelength range, although at much lower spectral resolution. In the present study the NiO* spectra observed in the laboratory are summarized and discussed. In addition, a preliminary spectral model of the NiO* emissions (Gattinger et

al., 2011a) is employed primarily to investigate the probable change in spectral shape when transferring the NiO* laboratory spectra, obtained at relatively high pressure, to the much lower pressures associated with the mesopause region.

Night airglow spectra recorded by two limb-viewing space-borne spectrographs on separate platforms are presented. The airglow spectra are corrected for atomic emissions and for the well-known molecular emission systems, mainly the Herzberg O_2 bands in the near-ultraviolet and blue regions, and the Meinel hydroxyl bands in the red spectral region. The residual observed spectra are then separated into NO_2^*, FeO* and NiO* components using a least squares fitting routine and their temporal variations are explored.

2 Laboratory observations of the chemiluminescent NiO* emission

The earliest observations of the NiO* emissions were recorded by Rosen (1945) who identified numerous spectral features and proposed a band classification scheme. Srdanov and Harris (1988) applied high resolution spectroscopic techniques to study the emissions in greater detail. These latter authors observed additional spectral features and proposed changes to the earlier band classifications. From a detailed spectral analysis Friedman-Hill and Field (1992) obtained accurate molecular constants for the NiO ground state and identified another NiO band system in the one micron region. Balfour et al. (2004) simplified the emission spectrum by cooling the emission source via an expansion jet and were able to identify additional bands, particularly those associated with the lowest ground state energy level. The observed rotationally resolved band spectra form a basic part of a new spectral model (Gattinger et al., 2011a) which is used in the present analysis. As some of the spectroscopic constants required to produce an accurate simulation are as yet unavailable it must be stressed the model is preliminary.

The dominant chemical reaction that produces NiO* in the mesopause region is expected to be

$$\mathrm{Ni} + \mathrm{O_3} \rightarrow \mathrm{NiO^*} + \mathrm{O_2} \qquad \text{(R1)}$$

with a bond energy for NiO of $373 \pm 3\,\mathrm{kJ\,mol^{-1}}$ (Watson et al., 1993), the exoergicity of Reaction (R1) is $266 \pm 4\,\mathrm{kJ\,mol^{-1}}$. Accordingly, the upper energy limit for the NiO* product is approximately $22\,600\,\mathrm{cm^{-1}}$, or 440 nm. This limit is in agreement with the laboratory observations of Burgard et al. (2006) (Fig. 1). The laboratory spectrum has been converted to photon units to compare with the space-borne observations discussed in the next section.

An independent laboratory spectrum of chemiluminescent NiO* arising from the $Ni + O_3$ reaction was obtained by Srdanov and Harris (1988). The spectral range extends from approximately 480 nm to 600 nm (Fig. 1) and the spectral resolution is considerably higher than for the Burgard et al. (2006) spectrum of NiO*. The two observed spectra in Fig. 1 form the basis of a "reference" NiO* spectrum used in the following sections to search for the presence of the NiO* spectral signature in the night airglow.

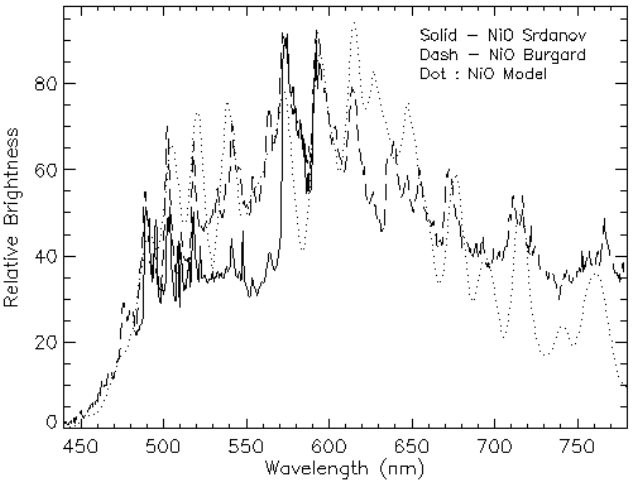

Fig. 1. A comparison of two laboratory spectra of chemiluminescent NiO* together with a preliminary spectral model simulation. The resolution of the Burgard spectrum in the visible region is approximately 5 nm.

The preliminary spectral model of the NiO* bands (Gattinger et al., 2011a) is also included in Fig. 1. This model spectrum has been convolved with a slit function for an approximate match to the resolution of the Burgard et al. (2006) spectrum. The primary function of the model in this study is to relate the laboratory NiO* observations made at relatively high pressures to the much lower pressure regime in the mesopause region. A similar study involving FeO* observations in the laboratory and in the airglow (Gattinger et al., 2011b) determined that the higher vibrational levels in the airglow are more heavily populated than those in the higher pressure laboratory observations. Accordingly, for the model comparison with laboratory spectra in Fig. 1 the lower vibrational levels in the excited NiO* states are assumed to be more heavily populated than the upper levels. With this assumption most of the prominent features observed in the two laboratory spectra are matched by the model spectrum. The extension of the NiO* model results appropriate to mesospheric pressures is discussed in the following sections.

Calculated Franck-Condon factors for the band systems included in the NiO* spectral model must also be considered preliminary due to the lack of accurate spectroscopic constants. Although individual relative band intensities will change with more accurate Franck-Condon factors it is expected that the overall distribution will remain similar and so have only a minor impact on the conclusions of the present study.

At instrumental resolutions typical for very faint airglow observations the spectrum in Fig. 1 will appear as a pseudo-continuum. This "continuum" is expected to be very faint,

thus making it difficult to detect in ground-based airglow spectra, which necessarily contain a strong non-atmospheric component (Sternberg and Ingham, 1972). Adding a further complication, the non-atmospheric component varies with galactic co-ordinates (Leinert et al., 1998). Consequently, data obtained with limb-viewing space-borne spectrographs are better suited to the task because of the airglow limb enhancement factor of at least fifty relative to the non-atmospheric background. A search for a spectral signature in night airglow space-borne observations which matches the chemiluminescent NiO* "continuum" is described in the following sections.

3 Night airglow continuum observations with the GLO-1 spectrograph

Limb-viewing spectra from the Arizona GLO-1 imaging spectrograph (Broadfoot et al., 1992; Broadfoot and Bellaire, 1999) are described here as part of the search for the NiO* signature in the night airglow. The GLO-1 instrument is a Space Shuttle-borne optical suite that included an imaging spectrograph with a spectral range from 120 to 900 nm and a spectral resolution that ranges from approximately 0.5 nm to 1 nm. In the current analysis the averaged GLO-1 night airglow tangent limb spectrum, shown in Panel A of Fig. 2, was obtained on mission STS 53, 2–12 December 1992 (Broadfoot and Bellaire, 1999). The altitude range for the averaged spectrum is from approximately 85 km to 95 km. Other spectra from this instrument have been used to study meteoric metals in the thermosphere (Gardener et al., 1999).

Following the procedures described by Evans et al. (2010), known airglow emission features were matched to the observed spectrum. These features included the Herzberg O_2 band systems, the Meinel OH bands, the O_2 Atmospheric bands and a number of atomic emission lines. The assembled matching simulated spectrum is shown in Panel B of Fig. 2. This model spectrum has been subtracted from the observed spectrum of Panel A to give the difference spectrum that is shown in Panel C of Fig. 2. This spectrum includes the "unidentified" features present in the GLO-1 night airglow spectrum. From Panel C the average residual tangent limb brightness over the 320 to 380 nm spectral range is approximately 2×10^7 photons $cm^{-2}\,s^{-1}\,nm^{-1}$. Converted to equivalent zenith viewing brightness, assuming a tangent limb enhancement factor of fifty, this is 4×10^5 photons $cm^{-2}\,s^{-1}\,nm^{-1}$, or 0.04 Rayleigh $Å^{-1}$. This is approximately an order of magnitude fainter than the ground-based continuum brightness observed by Broadfoot and Kendall (1968), and underlines the difficulty of searching for very faint continuum sources in ground-based spectra.

The residual "continuum" spectrum in Panel C of Fig. 2 shows a clear increase in brightness with increasing wavelength from approximately 440 nm to 550 nm. In Fig. 3 the residual continuum observed by the GLO-1 instrument

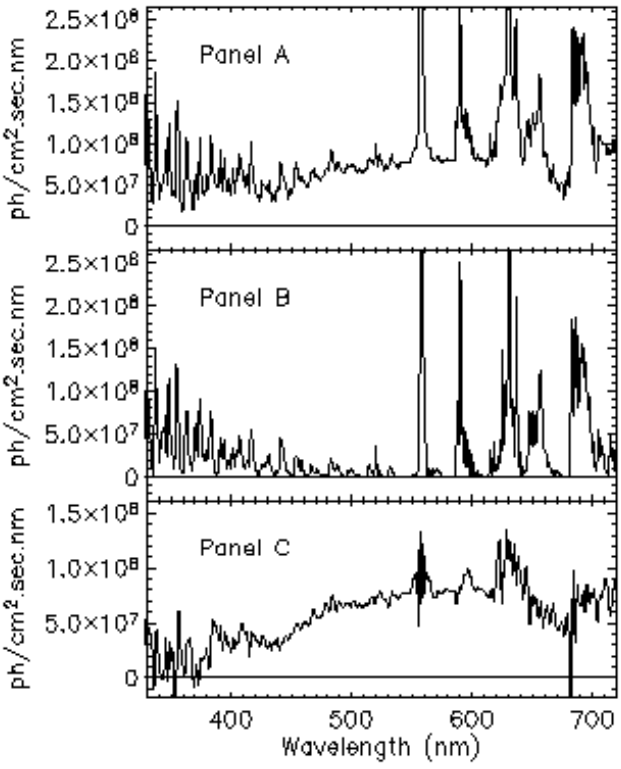

Fig. 2. (A) The averaged night airglow limb spectrum from the Arizona GLO-1 spectrograph on-board STS 53, approximately over the 85 km to 95 km altitude range. **(B)** Simulated night airglow spectrum to match the known spectral features in **(A)**. **(C)** Panel **(A)** observed spectrum minus panel **(B)** model spectrum. The difference spectrum is spectrally convolved with a 1.3 nm half width triangular function to improve figure clarity. Narrow spectral artifacts remain at the locations of the bright airglow atomic lines. The residual is a "continuum" with a broad peak near 600 nm.

(Panel C of Fig. 2) is compared with the NiO* model spectrum for laboratory pressure (Fig. 1) and the chemiluminescent NiO* model spectrum computed for mesospheric pressures. The spectral region beyond 620 nm has been omitted in order to stress the blue region. An average of the observed unexplained nearly uniform continuum between 380 nm to 430 nm, approximately 3×10^7 photons $cm^{-2}\,s^{-1}\,nm^{-1}$, has been subtracted from the residual spectrum over the whole wavelength range.

The mesospheric NiO* model spectrum threshold in the 450 nm region is located to the blue by approximately 20 nm compared with the model spectrum for laboratory pressure, guided by the observed blue threshold of the GLO-1 spectrum. In the present analysis, a wedge distribution (decreasing linear weights from 10 to 1) of vibrational level populations has been assumed for the laboratory pressures while a flat distribution of equal weights has been used to simulate the vibrational distribution at mesospheric pressures levels appropriate to the satellite observations. In the future,

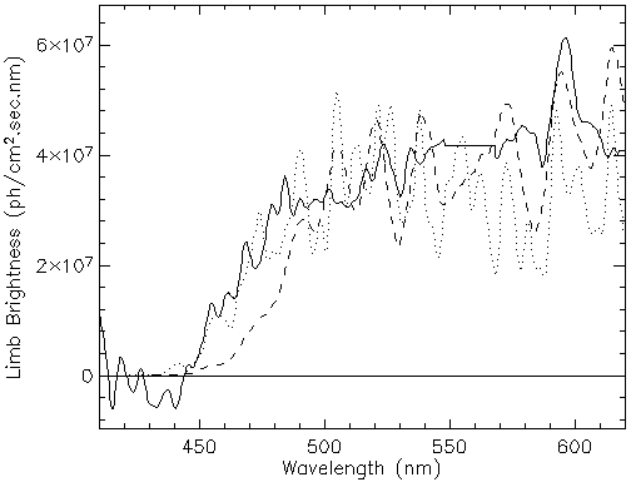

Fig. 3. Comparison between the GLO-1 observed airglow limb "continuum" (solid, from panel **(C)** of Fig. 2) and the NiO* model spectra for laboratory pressure (dash, from Fig. 1) and for mesospheric pressure (dot). The large noise spikes in the difference spectrum at OI 558 nm (panel **(C)** of Fig. 2) are replaced by a straight line.

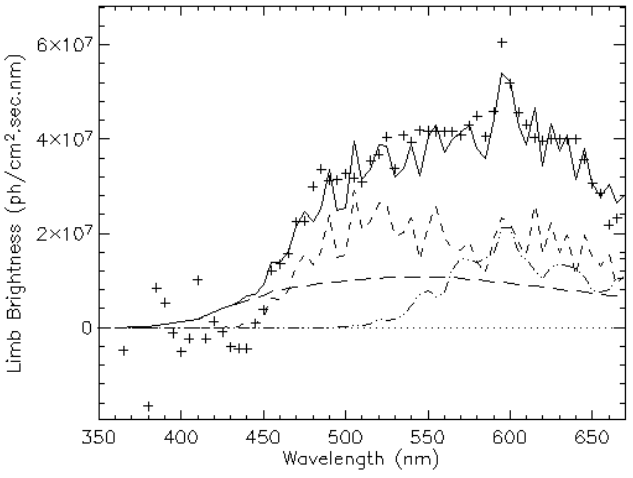

Fig. 4. Least-squares fit of the chemiluminescent FeO* model spectrum (dot-dot-dash), the NiO* model spectrum (short dash), the chemiluminescent NO_2^* emission (long dash), and the total (solid) to the GLO-1 observed airglow limb "continuum" from panel **(C)** of Fig. 2 (+ + +), all averaged over 5 nm intervals. The large noise spikes in the difference spectrum at OI 558 nm and OI 633 (panel **(C)** of Fig. 2) are replaced by straight lines. The ratio of NiO* to FeO* is 2.3 ± 0.2 and NO_2^* to FeO* is 1.3 ± 0.2, integrated over the full spectral range of Fig. 4.

valuable information could be obtained from rocket releases into the mesosphere that generate NiO* vapour trails using techniques similar to those employed by Best et al. (1972) to generate FeO* emissions.

Following the observations of Evans et al. (2010), the residual GLO-1 spectrum in Fig. 2, Panel C, is expected to include a component arising from mesospheric chemiluminescent FeO* emissions. Evans et al. (2010) built their analysis on the observation of FeO* in persistent meteor trains by Jenniskens et al. (2000). The FeO* component must be removed from the total residual continuum to isolate any previously unidentified features. Least squares combinations of the model mesospheric FeO* spectral profile (Gattinger et al., 2011b) and the model NiO* spectral profile (Gattinger et al., 2011a), along with the NO_2^* spectral profile (Becker et al., 1972; Gattinger et al., 2009) known to be present in varying amounts (McDade et al., 1986), are applied to the GLO-1 residual continuum in Fig. 4. Gattinger et al. (2010) found that at latitudes equatorward of 40°, commensurate with the current observations, the NO_2^* signature is faint relative to the more poleward night airglow NO_2^* brightness. The spectral region above 670 nm is omitted in order to avoid the excessive noise in the difference spectrum caused by the stronger OH bands towards the infrared. The NiO* to FeO* ratio, summed over the spectral region of Fig. 4, is 2.3 ± 0.2 as derived from the least squares procedure. The NiO* model threshold at 450 nm is well aligned spectrally with the observed threshold. The NO_2^* to FeO* ratio is 1.3 ± 0.2, also integrated over the full spectral range of Fig. 4. Again, it must be stressed that the model simulations are preliminary versions.

The mesospheric model spectrum in Fig. 4 contains features at 455 nm and 470 nm which correspond to transitions arising from upper levels centred on $v' = 5$ of the upper electronic state of the "blue" NiO* band systems. These relatively high vibrational levels observed in the airglow are in accord with the premise that NiO* is excited to high vibrational levels at mesospheric pressures. The brightness of the bands further towards the violet is constrained by the decreasing Franck-Condon factors for bands with larger vibrational quantum differences.

4 Night airglow continuum observations with the OSIRIS spectrograph

An analysis similar to that presented in the preceding section was completed for selected tangent limb night airglow observations made with the space-borne OSIRIS spectrograph (Llewellyn et al., 2004). The OSIRIS spectral range is from 274 nm to 815 nm with a resolution of approximately 1 nm. Individual spectra, recorded as the bore-sight repetitively scans the limb, are averaged over elapsed time to improve signal-to-noise. The OSIRIS spectra presented here are further averaged over latitudes in the Southern Hemisphere from the equator through to 40° South, intentionally omitting the more poleward regions to avoid the brighter NO_2^* emissions (Gattinger et al., 2010; Sheese et al., 2011).

An example of an average OSIRIS spectrum for June and July 2003 is shown in Panel A of Fig. 5. Only a portion of

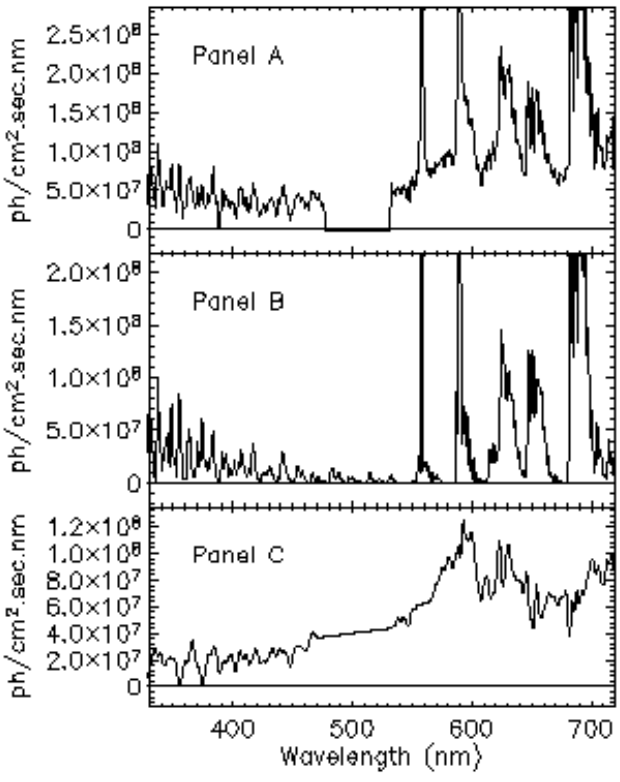

Fig. 5. (A) OSIRIS averaged tangent limb spectrum for June and July of 2003. The gap from 480 nm to 530 nm is the location of the OSIRIS spectral order sorter. **(B)** Simulated night airglow spectrum scaled to match **(A)** observed spectral features. **(C)** Residual spectrum (**A** minus **B**). The observed difference spectrum is spectrally convolved with a 2.5 nm half width triangular function to improve figure clarity. The data gap from 480 nm to 530 nm in **(C)** is filled assuming linear interpolation, and similarly for the strong OI 558 nm region.

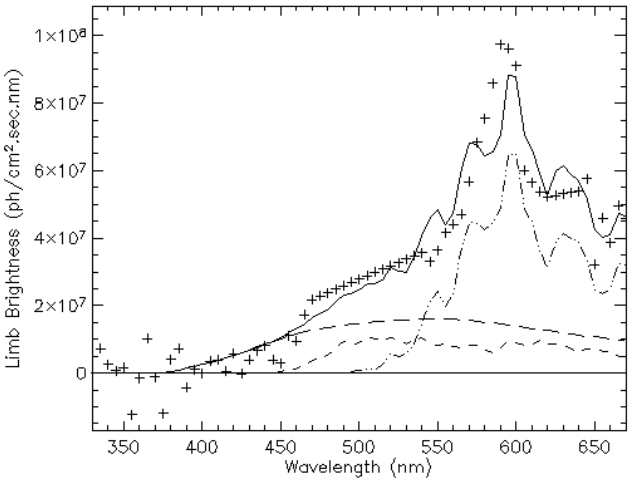

Fig. 6. Least-squares fitting of the chemiluminescent FeO* model spectrum (dot-dot-dash), the NiO* model spectrum (short dash), the chemiluminescent NO_2^* emission (long dash), and the total model spectrum (solid) versus the OSIRIS observed 85 km to 90 km averaged airglow limb "continuum" for June and July of 2003 (+ + +) (panel **(C)** of Fig. 5), all averaged over 5 nm intervals. The ratio of NiO* to FeO* is 0.3 ± 0.1 and NO_2^* to FeO* is 0.6 ± 0.1, integrated over the full spectral range of this figure.

the complete altitude range is included in this sample spectrum, namely from 85 km to 90 km. As in Fig. 2 for the GLO-1 observations, the matching simulated spectrum of the known airglow features, scaled to the observed OSIRIS average spectrum, is shown in Panel B of Fig. 5. The difference between the observed spectrum in Panel A and the simulated spectrum in Panel B is shown in Panel C of Fig. 5. This residual spectrum includes the "unidentified" features present in the OSIRIS night airglow spectrum.

It is apparent that the OSIRIS residual "continuum" spectrum of Panel C of Fig. 5 differs in spectral shape from the GLO-1 residual continuum shown in Panel C of Fig. 2. In particular the component arising from the FeO* chemiluminescent emission appears to be more prominent in the OSIRIS spectrum. This is addressed in a quantitative manner in Fig. 6 where a least-squares fitting of the spectral profiles of the NiO* and FeO* models for mesospheric pressure, plus the model chemiluminescent NO_2^* emission, is applied to resolve the three components present in the OSIRIS spectrum, as in Fig. 4 for the GLO-1 analysis. The resulting NiO* to FeO* ratio is 0.3 ± 0.1, integrated over the full spectral range of Fig. 6 as determined from the least squares fitting procedure. The NO_2^* to FeO* ratio is 0.6 ± 0.1.

Spectra from additional observing periods are included here to stress the variability of the "continuum" as observed by OSIRIS and to assist in evaluating the reliability of the analysis technique. Using the approach leading to Fig. 6, for the June and July period of 2004 (Fig. 7) the NO_2^* and NiO* features are present but fainter than in Fig. 6. For the June and July period of 2008 (Fig. 8) both the NiO* and NO_2^* features are absent with only the FeO* feature clearly present. Sheese et al. (2011) relate the inter-annual NO_2^* variability to solar cycle effects. The positive identification of spectral component changes in the OSIRIS data lends credence to the results shown in Fig. 6 where the FeO*, NiO* and NO_2^* emissions are all present.

In addition to the ratio variations demonstrated in the previous paragraphs, the brightness of the FeO* emission itself is known to vary by at least a factor of five (Evans et al., 2010 – their Fig. 3). These results exemplify the variability which should be expected in the FeO*, NiO* and NO_2^* emissions when searching for their signatures in the terrestrial night airglow. Photochemical models of the NiO* excitation processes, combined with models of FeO* production and loss (e.g. Plane, 2003) will need to address this variability. Possible sources and sinks are briefly discussed in the following section.

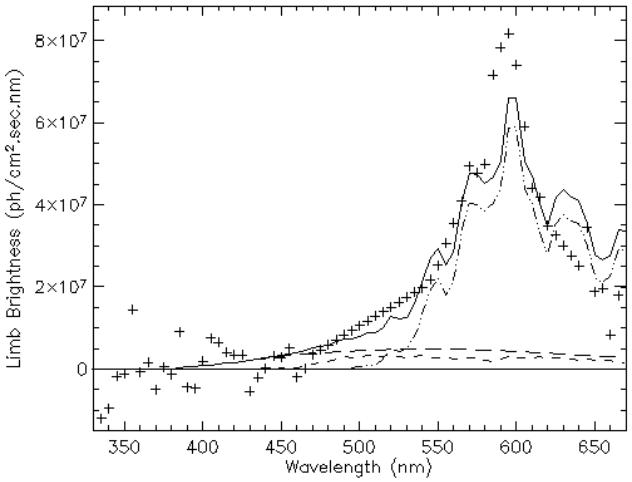

Fig. 7. Least-squares fitting of the chemiluminescent FeO* model spectrum (dot-dot-dash), the NiO* model spectrum (short dash), and the chemiluminescent NO_2^* emission (long dash), and the total model spectrum (solid) versus the OSIRIS observed airglow 85 km to 90 km averaged limb "continuum" for June and July of 2004 (+ + +), all averaged over 5 nm intervals. The ratio of NiO* to FeO* is 0.1 ± 0.1 and NO_2^* to FeO* is 0.2 ± 0.1, integrated over the full spectral range of Fig. 7.

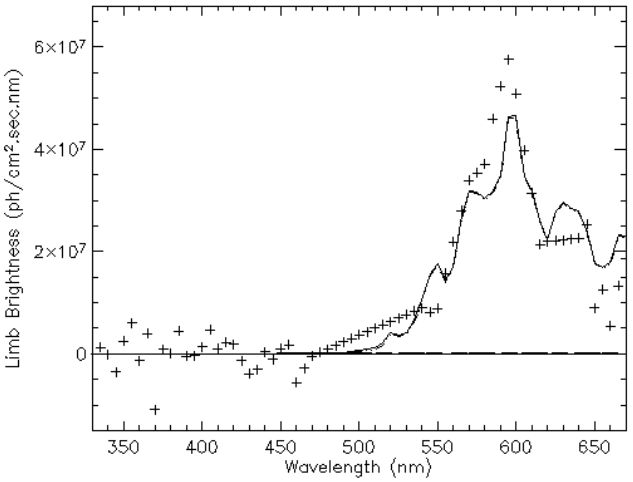

Fig. 8. Least-squares fitting of the chemiluminescent FeO* model spectrum (dot-dot-dash), the NiO* model spectrum (short dash), and the chemiluminescent NO_2^* emission (long dash), and the total model spectrum (solid) versus the OSIRIS observed airglow 85 km to 90 km averaged "continuum" for June and July of 2008 (+ + +), all averaged over 5 nm intervals. The ratio of NiO* to FeO* is 0.05 ± 0.05 and NO_2^* to FeO* is 0.0 ± 0.1, integrated over the full spectral range of Fig. 8. At the lowest tangent altitudes, near 80 km, there appears to be an additional unexplained emission source in the 380 to 420 nm region which impacts the NO_2^* component fit in each of years 2003, 2004 and 2008.

5 Chemiluminescent NiO* emission sources and sinks

Since both NiO* and FeO* emissions are excited in the laboratory by chemiluminescent reactions of Ni and Fe with ozone (Burgard et al., 2006), and since both metals have their source in meteorites, it is expected that NiO* would be an emission feature in the night airglow following the identification of FeO* (Evans et al., 2010; Saran et al., 2011). As with FeO* excitation, the catalytic cycle

$$Ni + O_3 \rightarrow O_2 + NiO^* \quad \text{(R2)}$$

$$NiO + O \rightarrow Ni + O_2 \quad \text{(R3)}$$

is expected to play a major role in Ni atmospheric chemistry. Like iron, the nickel atom is recycled and catalytically enhances the conversion of odd oxygen into O_2. Currently the rates for these two reactions do not appear to be available.

Typical altitude profiles of atomic iron have been determined with LIDAR measurements (Kane and Gardner, 1993a) to centre around 90 km. From the OSIRIS limb radiance observations for June and July of 2003, shown in Fig. 9, the NiO* and FeO* components present in the unidentified "continuum" described here also emanate from a similar altitude range. The altitude profiles are obtained by solving the least squares equation set (see previous section) at each altitude. Error bars are estimated based on the residuals between the sum of the least squares fit of the components and the observed "continuum" at each altitude. From these preliminary profiles the chemistry itself supports the thesis that the emission feature could be due to NiO*.

The analysis of the NiO*/FeO* ratio by the least squares method above has been successful in deriving the individual emission intensities of FeO* and NiO* from a number of spectra. There is considerable variability in the observed NiO* to FeO* emission ratio in the night airglow. Summarizing from the previous sections, the GLO-1 spectrum (Fig. 4) indicates an NiO* to FeO* ratio of approximately 2:1 while for the OSIRIS spectrum (Fig. 6) a ratio of approximately 1:3 is obtained. Additional OSIRIS spectra indicate an apparent lack of NiO* emission on occasion.

While we have no explanation for this ratio variation it is possibly in part due to the variability of the meteoritic metal influx ratios. There are two sources of atmospheric nickel from meteorites, ablation of meteors and sedimentation of cosmic dust (Hemenway and Hallgren, 1970). Taenite (Fe, Ni) is a mineral found naturally on Earth mostly in iron meteorites (Albertson et al., 1978); it is an alloy of iron and nickel with nickel proportions ranging from 20 % up to as high as 65 %. Typically, most meteorites have lower Ni/Fe ratios, around 6 % (Brown and Patterson, 1947). The elemental composition analysis of 200 samples of stratospheric dust (Jessberger et al., 2001) indicated that the ratio of atomic Ni/Fe in cosmic dust is near 80 %. The different sources of meteoritic metals have been reviewed by Rietmeijer (2000).

Ablation from meteors maximizes between 85 km and 90 km (Kane and Gardner, 1993b), at times from meteors

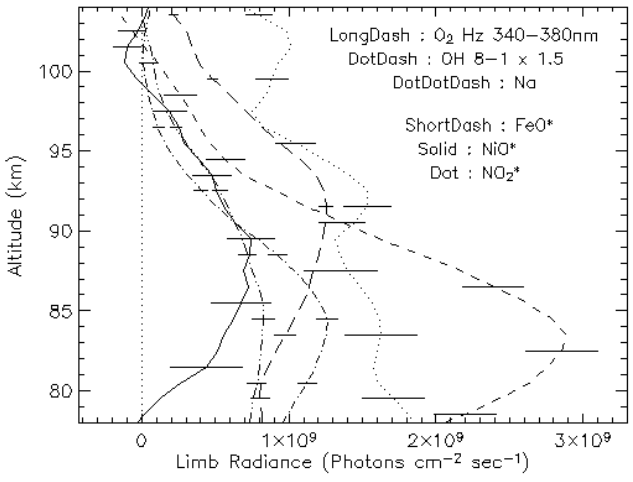

Fig. 9. Observed night airglow limb radiances obtained from averaged OSIRIS spectra, June and July of 2003. The O_2 Hz, OH and Na curves are the scaled amounts used to form the airglow spectrum subtracted at each altitude, e.g. panel **(B)** of Fig. 5. The FeO*, NiO* and NO_2^* curves are from the least squares fitting routine as applied to the residual continuum at each altitude, e.g. panel **(C)** of Fig. 5. Only those emissions within the spectral range of Fig. 6 are included in the limb radiance sums. For the NiO* emission the equivalent zenith differential brightness as detected from ground observations would be approximately 0.1 Rayleigh per nm, or 0.01 Rayleigh per Ångstrom.

that have high Ni/Fe ratios (Schramm et al., 1989) that originate from the cores of planetoids, the annual Leonids shower in November is one example. The GLO-1 spectrum shown in Fig. 4 was taken during the period from 2–11 December 1992. This immediately precedes the maximum of the GEMINID meteor shower, which is centered on 13 December (Lokanadham et al., 2010), and follows the Leonids shower of 17 November, a shower with highly variable rates (Brown, 1999) with a periodicity of 33 yr. However, while Gardner et al. (2005) did observe a seasonal variation in Fe concentration at mid-latitudes, there was no clear indication of a temporal correlation with the occurrence of meteor showers.

An additional factor influencing emission sources and sinks is the complex altitude distribution of mesospheric and thermospheric metals arising from meteor deposition (Gardner et al., 1999). The profiles of Fe^+ measured with mass spectrometers on rocket flights suggest that the sedimentation cosmic dust source is significant from 80 km to above 120 km (Grebowsky and Aikin, 2002). This is further supported by lidar measurements of atomic sodium, which demonstrate an ablation profile superimposed on a much broader altitude background profile (Lokanadham et al., 2010). Differences in meteor ablation rates (Vondrak et al., 2008), and sink mechanisms (Plane, 2003), could also have a significant impact.

Another possible reason for the NiO* to FeO* ratio variability might be significant differences in the luminous efficiency of the reaction products. West and Broida (1975) estimated a 2 % to 6 % production efficiency of FeO* from $Fe + O_3$. Extrapolating their laboratory measurements taken at two relatively high pressures to the much lower mesospheric pressures suggests that this efficiency could increase considerably above 6 %. Currently there does not appear to be a quantitative laboratory measurement of the analogous NiO* production efficiency.

6 Summary

The discovery of a chemiluminescent FeO* emission feature in OSIRIS/Odin spectra of the night airglow near 87 km has raised interest in other meteorite metallic emissions in the airglow. Since the meteorite source of atomic metals in the mesosphere contains both iron and nickel, with Ni being typically 6 % of Fe, it is expected that faint emissions involving Ni should also be present in the night airglow. A new spectral model has been used to model the laboratory observations of chemiluminescent NiO* emissions and then to search for the signature of NiO* in satellite measurements of the night airglow. A faint, previously unidentified, "continuum" extending longwave of 440 nm has been identified in night airglow spectra obtained from two space-borne limb viewing instruments. From a comparison with laboratory spectra this continuum is identified as arising from the NiO* emission. A simultaneous least-squares fit for the NiO*, FeO* and NO_2^* spectral profiles was conducted on Shuttle GLO and OSIRIS satellite observations of visible airglow spectra. The observed ratio of NiO*/FeO* is 2.3 ± 0.2 from the GLO experiment and from 0.05 ± 0.05 to 0.3 ± 0.1 for the OSIRIS observations. The similarity of the altitude profiles of the NiO* and FeO* emissions also suggests that the new airglow emission is NiO* since both chemiluminescent oxides can originate from atomic reactions with ozone. Possible causes of this observed ratio variation are briefly discussed.

Acknowledgements. This work was supported by the Canadian Space Agency and the Natural Sciences and Engineering Research Council (Canada). Odin is a Swedish-led satellite project funded jointly by Sweden (SNSB), Canada (CSA), France (CNES) and Finland (Tekes). Funding for the Shuttle flight and the GLO-1 instrument came from NASA and USAF Phillips Laboratory.

Edited by: W. Ward

References

Albertsen, F., Knudsen, J. M., and Jensen, G. B.: Structure of taenite in two iron meteorites, Nature, 273, 453–454, 1978.

Ångström, A. J.: Spektrum des nordlichts, Pogg. Ann., 137, 161–163, 1869.

Balfour, W. J., Cao, J., Jensen, R. H., and Li, R.: The spectrum of nickel monoxide between 410 and 510 nm: laser-induced fluorescence and dispersed fluorescence measurements, Chem. Phys. Lett., 385, 239–243, 2004.

Becker, K. H., Groth, W., and Thran, D.: The mechanism of the air-afterglow NO+O→NO_2+hv, Chem. Phys. Lett., 15, 215–220, 1972.

Best, G. T., Forsberg, C. A., Golomb, D., Rosenberg, N. W., and Vickery, W. K.: The release of iron carbonyl into the upper atmosphere, J. Geophys. Res., 77, 1677–1680, 1972.

Broadfoot, A. L. and Bellaire, P. J.: Bridging the gap between ground-based and space-based observations of the night airglow, J. Geophys. Res., 104, 17127–17138, 1999.

Broadfoot, A. L. and Kendall, K. R.: The airglow spectrum, 3100–10000 Å, J. Geophys. Res., 73, 426–428, 1968.

Broadfoot, A. L., Sandel, B. R., Knecht, D., Viereck, R., and Murad, E.: A panchromatic spectrograph with supporting monochromatic imagers, Appl. Opt., 31(16), 3083–3096, 1992.

Brown, P.: The Leonid Meteor Shower: Historical Visual Observations, Icarus, 138, 287–308, 1999.

Brown, H. and Patterson, C.: The Composition of Meteoritic Matter: II. The Composition of Iron Meteorites and of the Metal Phase of Stony Meteorites, J. Geol., 55, 508–510, 1947.

Burgard, D. A., Abraham, J., Allen, A., Craft, J., Foley, W., Robinson, J., Wells, B., Xu, C., Stedman, D. H.: Chemiluminescent reactions of nickel, iron and cobalt carbonyls with ozone, Appl. Spectrosc., 60, 99–102, 2006.

Evans, W. F. J., Gattinger, R. L., Slanger, T. G., Saran, D. V., Degenstein, D. A., and Llewellyn, E. J.: Discovery of the FeO orange bands in the terrestrial night airglow spectrum obtained with OSIRIS on the Odin spacecraft, Geophys. Res. Lett., 37, L22105, doi:10.1029/2010GL045310, 2010.

Friedman-Hill, E. J. and Field, R. W.: Analysis of the [16.0] $^3\Sigma^- - X^3\Sigma^-$ and [16.0]$^3\Sigma^-$-[4.3]$^3\Pi_i$ band systems of the NiO molecule, J. Mol. Spectrosc., 155 (2), 259–276, doi:10.1016/0022-2852(92)90516-Q, 1992.

Gardner, C. S., Plane, J. M. C., Pan, W. L., Vondrak, T., Murray, B. J., and Chu, X. Z.: Seasonal variations of the Na and Fe layers at the South Pole and their implications for the chemistry and general circulation of the polar mesosphere, J. Geophys. Res., 110, D10302, doi:10.1029/2004JD005670, 2005.

Gardner, J. A., Broadfoot, A. L., McNeil, W. J., Lai, S. T., and Murad, E.: Analysis and modeling of the GLO-1 observations of meteoric metals in the thermosphere, J. Atmos. Solar-Terr. Phys., 61, 545–562, doi:10.1016/S1364-6826(99)00013-9, 1999.

Gattinger, R. L., Evans, W. F. J., McDade, I. C., Degenstein, D. A., and Llewellyn, E. J.: Observation of the chemiluminescent NO+O→NO_2+hν reaction in the upper mesospheric dark polar regions by OSIRIS on Odin, Can. J. Phys., 87, 925–932, doi:10.1139/P09-051, 2009.

Gattinger, R. L., McDade, I. C., Alfaro Suzán, A. L., Boone, C. D., Walker, K. A., Bernath, P. F., Evans, W. F. J., Degenstein, D. A., and Llewellyn, E. J.: NO_2 air afterglow and O and NO densities from Odin-OSIRIS night and ACE-FTS sunset observations in the Antarctic MLT region, J. Geophys. Res., 115, D12301, doi:10.1029/2009JD013205, 2010.

Gattinger, R. L., Evans, W. F. J., and Llewellyn, E. J.: Chemiluminescent NiO* emissions: Band systems and spectral simulation, Can. J. Phys., 89, 869–874, doi:10.1139/p11-068, 2011a.

Gattinger, R. L., Evans, W. F. J., Degenstein, D. A., and Llewellyn, E. J.: A spectral model of the FeO orange bands with a comparison between a laboratory spectrum and a night airglow spectrum observed by OSIRIS on Odin., Can. J. Phys., 89, 239–248, doi:10.1139/P11-003, 2011b.

Grebowsky, J. M. and Aikin, A. C.: In Situ Measurements of Meteoric Ions, in: Meteors in the Earth's Atmosphere, edited by: Murat, E. and Williams, I. P., Cambridge University Press, Cambridge, UK, 189–214, 2002.

Hemenway, C. L. and Hallgren, D. S.: The Variation of the Altitude Distribution of the Cosmic Dust Layer in the Upper Atmosphere, Space Res., 10, 272–280, 1970.

Jenniskens, P., Lacey, M., Allan, B. J., Self, D. E., and Plane, J. M. C.: FeO "orange arc" emission detected in optical spectrum of Leonid persistent train, Earth, Moon and Planets, 82–83, 429–434, 2000.

Jessberger, E. K., Stephan, T., Rost, D., Arndt, P., Maetz, M., Stadermann, F. J., Brownlee, D. E., Bradley, J. P., and Kurat, G.: Properties of Interplanetary Dust: Information from Collected Samples, from "Interplanetary Dust", edited by: Grün, E., Gustafson, B. A. S., Dermott, S., and Fechtig, H., Springer Verlag, 509–567, 2001.

Kane, T. J. and Gardner, C. S.: Structure and seasonal variability of the nighttime mesospheric Fe layer at midlatitudes, J. Geophys. Res. 98, 16875–16886, 1993a.

Kane, T. J. and Gardner, C. S.: LIDAR observations of the meteoritic deposition of mesospheric metals, Science, 259, 1297–1300, 1993b.

Leinert, Ch., Bowyer, S., Haikala, L. K., Hanner, M. S., Hauser, M. G., Levasseur-Regourd, A.-Ch., Mann, I., Mattila, K., Reach, W. T., Schlosser, W., Staude, H. J., Toiler, G. N., Weiland, J. L., Weinberg, J. L., and Witt, A. N.: The 1997 reference of diffuse night sky brightness, Astron. Astrophys. Suppl. Ser., 127, 1–99, doi:10.1051/aas:1998105, 1998.

Llewellyn, E. J., Lloyd, N. D., Degenstein, D. A., Gattinger, R. L., Petelina, S. V., Bourassa, A. E., Wiensz, J. T., Ivanov, E. V., McDade, I. C., Solheim, B. H., McConnell, J. C., Haley, C. S., von Savigny, C., Sioris, C. E., McLinden, C. A., Griffioen, E., Kaminski, J., Evans, W. F. J., Puckrin, E., Strong, K., Wehrle, V., Hum, R. H., Kendall, D. J. W., Matsushita, J., Murtagh, D. P., Brohede, S., Stegman, J., Witt, G., Barnes, G., Payne, W. F., Piché, L., Smith, K., Warshaw, G., Deslauniers, D.-L., Marchand, P., Richardson, E. H., King, R. A., Wevers, I., McCreath, W., Kyrölä E., Oikarinen, L., Leppelmeier, G. W., Auvinen, H., Mégie, G., Hauchecorne, A., Lefèvre, F., de La Nöe, J., Ricaud, P., Frisk, U., Sjoberg, F., von Schéele, F., and Nordh, L.: The OSIRIS Instrument on the Odin Spacecraft, Can. J. Phys., 82, 411–422, 2004.

Lokanadham, B., Chandra, N. R., Rao, S. V. B., Raghunath, K., and Yellaiah, G.: Mesospheric sodium over Gadanki during GEMINID meteor shower 2007, Indian J. Radio Space Phys., 39, 7–10, 2010.

McDade, I. C., Llewellyn, E. J., Greer, R. G. H., and Murtagh, D. P.: ETON 3: Altitude profiles of the nightglow continuum at green and near infrared wavelengths, Planet. Space Sci., 34, 801–810, 1986.

McNeil, W. J., Lai, S. T., and Murad, E.: Differential ablation of cosmic dust and implications for the relative abundances of atmospheric metals, J. Geophys. Res., 103, 10899–10911, 1998.

Plane, J. M. C.: Atmospheric chemistry of meteoric metals, Chem. Rev., 103, 4963–4984, 2003.

Rietmeijer, F. J. M.: Interrelationships among meteoric metals, meteors, interplanetary dust, micrometeorites, and mete-

orites, Meteor. Planet. Sci., 35, 1025–1041, doi:10.1111/j.1945-5100.2000.tb01490.x, 2000.

Rosen, B.: Spectra of diatomic oxides by the method of exploded wire, Nature, 156, 570–570, 1945.

Saran, D. V., Slanger, T. G., Feng, W., and Plane, J. M. C.: FeO emission in the mesosphere: Detectability, diurnal behavior, and modeling, J. Geophys. Res., 116, D12303, doi:10.1029/2011JD015662, 2011.

Schramm, L. S., Brownlee, D. E., and Wheelock, M. M.: Major element composition of stratospheric micrometeorites, Meteoritics, 24, 99–112, 1989.

Srdanov, V. I. and Harris, D. O.: Laser spectroscopy of NiO: The $^3\Sigma^-$ ground state, J. Chem. Phys., 89, 2748–2753, doi:10.1063/1.455711, 1988.

Sheese, P. E., Gattinger, R. L., Llewellyn, E. J., Boone, C., and Strong, K.: Nighttime nitric oxide densities in the Southern hemisphere mesosphere – lower thermosphere, Geophys. Res. Lett., 38, 38, L15182, doi:10.1029/2011GL048054, 2011.

Sternberg, J. R. and Ingham, M. F.: Observations of the airglow continuum, Mon. Not. Roy. Astr. Soc., 159, 1–20, 1972.

Vondrak, T., Plane, J. M. C., Broadley, S., and Janches, D.: A chemical model of meteoric ablation, Atmos. Chem. Phys., 8, 7015–7031, doi:10.5194/acp-8-7015-2008, 2008.

Watson, L. R., Thiem, T. L., Dressler, R. A., Salter, R. H., and Murad, E.: High temperature mass spectrometric studies of the bond energies of gas-phase zinc oxide, nickel oxide, and copper(II) oxide, J. Phys. Chem., 97(21), 5577–5580, doi:10.1021/j100123a020, 1993.

West, J. B. and Broida, H. P.: Chemiluminescence and photoluminescence of diatomic iron oxide, J. Chem. Phys., 62, 2566–2574, 1975.